Chinese Chemical Letters 33 (2022) 5196–5199

Contents lists available at ScienceDirect

Chinese Chemical Letters

journal homepage: www.elsevier.com/locate/cclet

Electrocatalytic degradation of pesticide micropollutants in water by high energy pulse magnetron sputtered Pt/Ti anode

Yuxin Zeng[a], Siyao Zhang[a], Lifeng Yin[a,*], Yunrong Dai[b,*]

[a] School of Environment, Beijing Normal University, Beijing 100875, China
[b] School of Water Resources and Environment, China University of Geosciences (Beijing), Beijing 100083, China

ARTICLE INFO

Article history:
Received 7 September 2021
Revised 8 December 2021
Accepted 13 January 2022
Available online 17 January 2022

Keywords:
Electrocatalysis
Magnetron sputtering
Pesticide
Degradation mechanism
Dichlorvos
Azoxystrobin

ABSTRACT

The increasing occurrence of pesticide micropollutants highlights the need for innovative water treatment technologies, particularly for small-community and household applications. Electro-oxidation is being widely studied in this area, unfortunately, safe, stable and efficient electrocatalytic anodes without released heavy metal ions are still highly required. In this study, we fabricated a Pt/Ti anode by high energy pulse magnetron sputtering (HiPIMS-PtTi) which was used to decompose dichlorvos (DDVP) and azoxystrobin (AZX) in water. The results show that the reaction rate constant (k_{ENR}) on HIPIMS was 35.7 min^{-1} (DDVP) and 41.3 min^{-1} (AZX), respectively, superior to electroplating Pt/Ti anode (EP-PtTi). The identification of radicals ($^{\bullet}OH$, $^1O_2$, $^{\bullet}O_2^-$) and micro-area analyses evidenced that Pt atoms were embedded into the TiO_2 lattice on the surface of Ti plate by high-energy ions, which resulted in more adsorbed hydroxyls, and higher production of $^{\bullet}OH$ under polarization conditions. Besides, the electro-oxidation intermediates of DDVP and AZX were identified and the degradation pathways were speculated: (1) indirect oxidation dominated by $^{\bullet}OH$ attack, and (2) direct electron transfer reaction of pesticides on the anode surface. The cooperated reactions achieve the complete degradation and highly efficient mineralization of DDVP and AZX.

The increasing usage of pesticides in the field of agricultural cultivation has been found to be a significant risk to water supplies [1,2]. More than 90% of pesticides used are released to the aqueous environment by leaching and surface runoff [3]. For examples, the residues of organophosphorus pesticides such as dichlorvos (DDVP) may lead to respiratory failure, delayed neuropathy and endocrine disorders [4]. More than 70% of strobilurins pesticides such as azoxystrobin (AZX) were leached into the environment by rainfall, posing a potential threat to human health and the ecological environment [5]. Pesticide residues can accumulate along with food chain, which may cause a long-lasting effect on ecosystems [6]. Closely related to daily life, it is difficult to completely remove pesticide residues on the surface of vegetables and fruits by rinsing. Therefore, how to rapidly and efficiently clarify the pesticide residues and eliminate the threat to human health is an important scientific issue.

Electrocatalysis has been widely applied to treat the pesticide-contaminated water [7–10]. The removal efficiency of boron-doped diamond (BDD) anode for various pesticides can reach above 90% [11–14]. Dimensionally stable anodes (DSA), such as Ti/SnO_2-Sb/Ce-PbO_2 anode, can also degrade 2,4,5-trichlorophenoxyacetic acid and benzophenone effectively [15–18]. Unfortunately, BDD anode is too expensive for practical application. As for traditional DSA anode, the Sn^{4+}, Pb^{2+}, Sb^{3+} and other non-noble metal ions are potentially released from the surface and lead to the secondary pollutions and health problems [19–21]. By contrast, noble metal anodes (NMAs) take advantage of low toxicity, high conductivity, and oxidation resistance [21–23]. Among NMAs, Pt/Ti composite anodes are used more on laboratory due to strong tolerance and high plasticity [24,25]. However, the traditional electroplating Pt/Ti anodes usually have low efficiency and short lifetime, which is caused by the weak binding between Pt and Ti substrate [26,27]. Generally, the Pt/Ti anodes will lose their electrocatalytic activity in several weeks, even in several days under the actual working conditions.

In this study, we fabricated Pt/Ti anodes by high energy pulse magnetron sputtering (HiPIMS-PtTi), and electroplating processes (EP-PtTi) as a comparison (Materials and methods in Supporting information), and named them after their processing time (min). The surface structures of four Ti-based modified anodes were observed under scanning electron microscope (SEM, Fig. S2 in Supporting information). The surfaces of HiPIMS-PtTi30 and HiPIMS-

* Corresponding authors.
E-mail addresses: lfyin@bnu.edu.cn (L. Yin), Daiyr@cugb.edu.cn (Y. Dai).

https://doi.org/10.1016/j.cclet.2022.01.031
1001-8417/

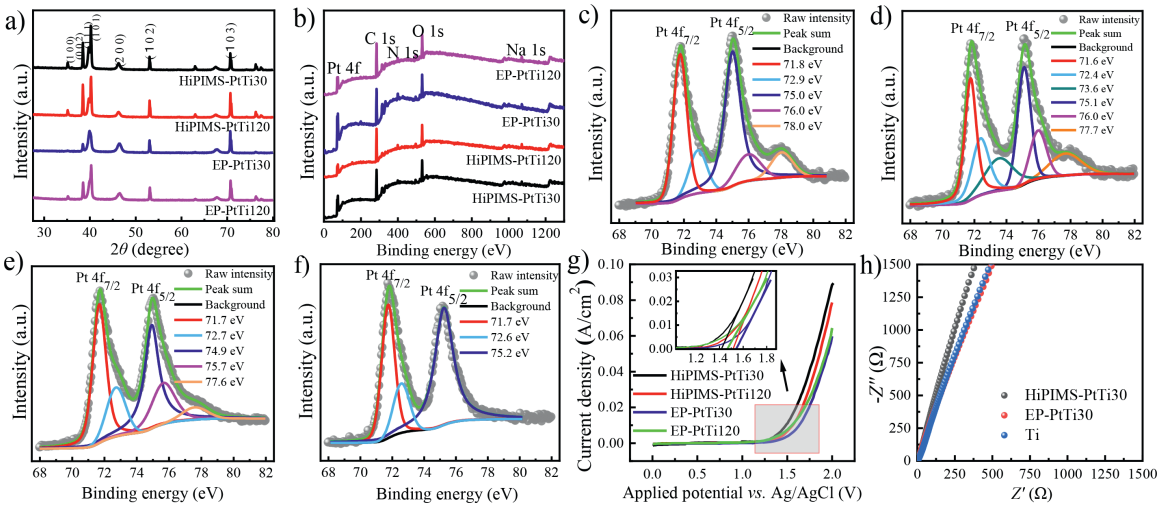

Fig. 1. (a) HiPIMS-PtTi30, HiPIMS-PtTi120, EP-PtTi30, EP-PtTi120 anode X-ray diffraction spectrum. (b) The low-resolution X-ray photoelectron full spectrum of four anodes. The high-resolution Pt 4f spectrum of HiPIMS-PtTi30 (c), HiPIMS-PtTi120 (d), EP-PtTi30 (e) and EP-PtTi120 (f). (g) Linear voltammogram of four electrodes. (h) Impedance spectrum of HiPIMS-PtTi30, EP-PtTi30 and Ti electrodes.

PtTi120 prepared by magnetron sputtering show more ravines and gullies. The uneven structures are obviously generated by the oxalic acid etching of Ti plate. The Pt/Ti anode prepared by HiPIMS is still a pristine place. In other words, the HiPIMS results in the Pt atoms implanted into the crystalline of the Ti plates and integrated with them together to improve the adhesion between the coating and the substrate, and thus ensures the coating attached tightly to the metal surface [28,29]. While the EP-PtTi30 and EP-PtTi120 prepared by electroplating show smoother surfaces. More particles and compact structures were observed. Based on the statistical calculation of the surface particle size, it is found that the particle sizes of HiPIMS-PtTi30 are 5–10 nm, and the average size is about 7 nm. While the particles on HiPIMS-PtTi120 are similar but bigger, with an average size of 8.5 nm. As for EP-PtTi30 and EP-PtTi120, the average particle size is about 15 nm and 18 nm, respectively.

The crystal structures of four anodes were investigated by X-ray diffraction (XRD, Fig. 1a). The diffraction peaks at 2θ = 35.1°, 38.4°, 40.2°, 53.0° and 70.7° correspond to the (110), (101), (200), (102) and (103) crystal planes of Ti. The diffraction peaks of HiPIMS-PtTi30 and HiPIMS-PtTi120 anodes at 2θ = 39.9° and 46.4° correspond to the (111) and (201) crystal planes of Pt, respectively, with the spacing distances of 0.226 nm and 0.196 nm. As shown in Fig. 1a, the Pt coatings grow along with the (111) crystal plane orientation, indicating typical face-centered cubic crystals were formed on four anodes [4,5]. The Pt on HiPIMS-PtTi30, HiPIMS-PtTi120, EP-PtTi30 and EP-PtTi120 were identified as PDFs #89–7382, 70–2057, 87–0640 and 87–0640, respectively, indicating that the Pt crystal structures were slightly different. The average diameters of Pt particles in HiPIMS-PtTi30, HiPIMS-PtTi120, EP-PtTi30 and EP-PtTi120 anodes are 5.7 nm, 8.4 nm, 13.5 nm and 20.2 nm, respectively, calculated by Scherrer formula and half peak width of Pt(111) diffraction peak. These results are consistent with that of SEM. The size of Pt particles prepared by electroplating was larger than that by magnetron sputtering. Under a high current density, the cathodic polarization will be enhanced, so the sizes of Pt particle are reinforced [30].

The X-ray photoelectron spectroscopies (XPS) of four Pt/Ti anodes are shown in Fig. 1b. It is also inferred that Pt was uniformly loaded onto the surface of Ti matrix, forming a stable metal coating [31]. The Pt on four anode surfaces was further critically scanned and fitted by deconvolution, as shown in Figs. 1c-f. The Pt 4f binding energies corresponding to the two maximum absorption peaks of HiPIMS-PtTi30 anode are 71.8 eV and 75.0 eV, respectively. The binding energies of metallic Pt are mainly 71.7–71.9 eV ($4f_{7/2}$) and 74.8–75.0 eV ($4f_{5/2}$), while those of oxidized Pt are higher [32]. Therefore, it can be concluded that the main existing form of Pt in HiPIMS-PtTi30 anode is the metallic state. Comparing the peak positions of Pt 4f prepared by two methods (Table S3 in Supporting information), the $4f_{7/2}$ peaks in HiPIMS-PtTi30 and HiPIMS-PtTi120 are split into duet and triplet, and slightly redshift, which may be due to the Pt particles on the HiPIMS-PtTi surface prepared by magnetron sputtering had higher dispersion and were partially oxidized [32,33].

The oxygen evolution potentials (OEP) of four anodes were tested by linear voltammetry. The linear sweep voltammetry (LSV) curves were obtained under the scanning voltage range of 0–2.0 V, as shown in Fig. 1g. The OEPs of HiPIMS-PtTi30, HiPIMS-PtTi120, EP-PtTi30 and EP-PtTi120 were 1.42 V, 1.48 V, 1.52 V, and 1.55 V (*vs.* Ag/AgCl), respectively. The higher OEP effectively expands potential windows for the degradation of organic pesticides in water [34–36]. The similarly OEPs indicated that the ability of these four electrodes to occur oxygen evolution side reaction is equivalent. Meanwhile, Fig. 1h shows that the impedance values of three electrodes are low, indicating that the conductivity of HiPIMS-PtTi30 and EP-PtTi30 are good.

The degradation of DDVP and AZX on different Pt/Ti anodes was evaluated as shown in Fig. 2. On HiPIMS-PtTi30 anode, removal efficiency of DDVP and AZX reached 88.2% and 91.7% respectively within 1 h. By applying pseudo-first-order kinetics model (Eq. S1 in Supporting information), the removal kinetics of AZX and DDVP by four anodes shows significant linear relationship (Figs. 2b and d). As shown in Table S4 (Supporting information), the degradation efficiency constant (k_{ENR}) on HiPIMS-PtTi30 for DDVP is 35.7 min^{-1}, which is 2.04, 1.59 and 2.46 times of HiPIMS-PtTi120, EP-PtTi30 and EP-PtTi120, respectively. The k_{ENR} on HiPIMS-PtTi30 for AZX is 41.3 min^{-1}, which is 3.36, 1.07 and 3.47 times of HiPIMS-PtTi120, EP-PtTi30 and EP-PtTi120, respectively. Furthermore, HiPIMS-PtTi30 possesses the highest quantum efficiency for the degradation of pesticides, which is consistent with the results of the above discussion (Table S5 in Supporting information).

The effects of pH on the degradation of DDVP ($[DDVP]_0$ = 10 mg/L) by HiPIMS-PtTi30 were investigated at pH 2.0, 4.0, 7.0, 8.0 and 10.0. The DDVP degradation efficiency was measured and fitted by first-order kinetics. The results are shown in Figs. 2e and f. At pH 4.0, k_{ENR} is the highest (35.5 min^{-1}),

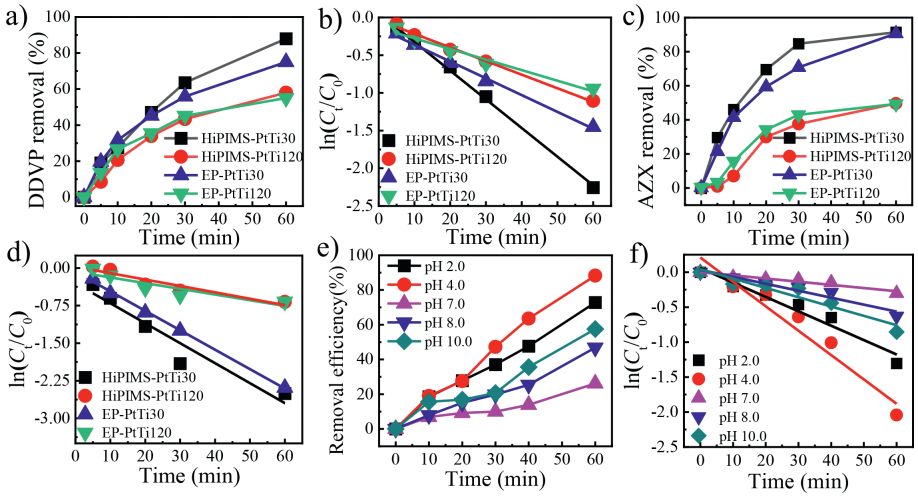

Fig. 2. Electrocatalytic degradation of DDVP (a, b) and AZX (c, d) on HiPIMS-PtTi30, HiPIMS-PtTi120, EP-PtTi30, EP-PtTi120, and the effects of pH on degradation of DDVP (e, f) on HiPIMS-PtTi30. Current density 60 mA/cm^2; [Na_2SO_4] = 22.5 mmol/L, d = 2 mm, $[DDVP]_0$ and $[AZX]_0$ 10 mg/L; reaction volume: 500 mL.

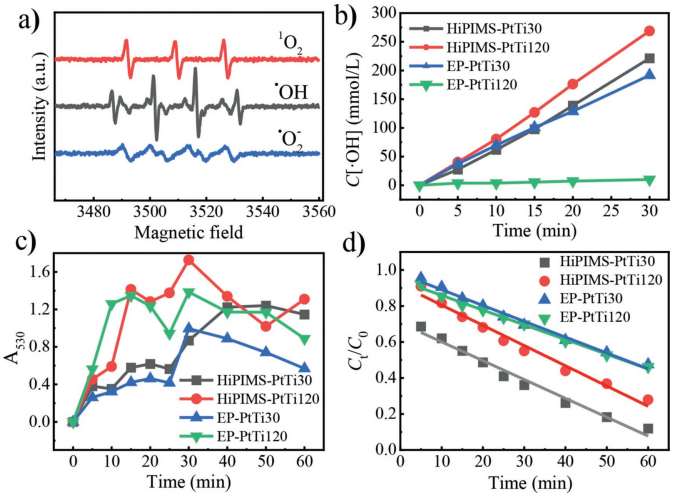

Fig. 3. (a) Electron spin resonance detection results of ROS. The law of ·OH (b), $·O_2^-$ (c) and $^1O_2$ (d) production on four anodes.

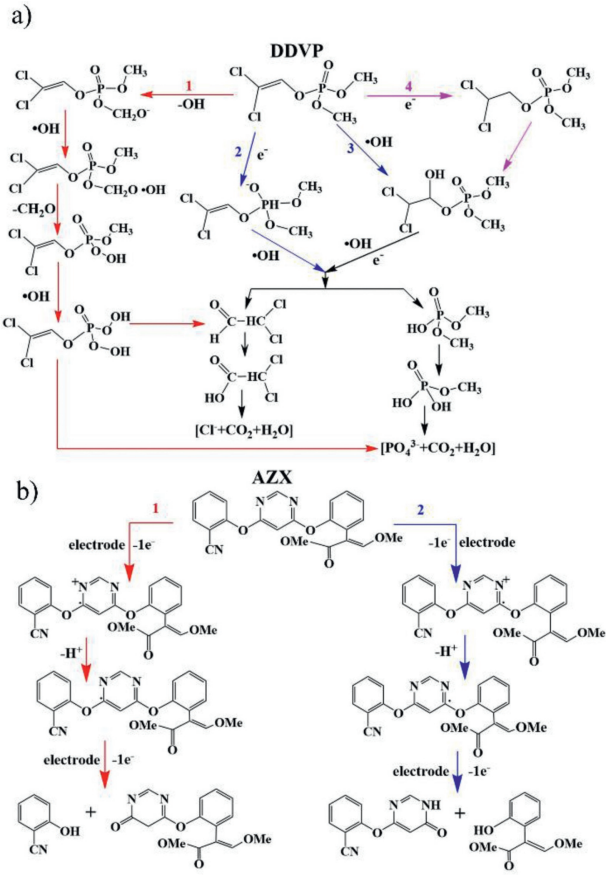

Fig. 4. Potential reaction pathway of DDVP (a) and AZX (b) in electrocatalytic system.

which is 7.8 times higher than that under neutral conditions (Table S6 in Supporting information). This may be due to the reinforced oxidizability of ·OH under acidic conditions [37–39]. However, when pH value is too low, the formation of ·OH will be suppressed [40,41] and the high concentration of H^+ may result in side reaction of hydrogen evolution (HER) [42]. At pH 8.0 and 10.0, k_{ENR} are 9.98 and 13.5 min^{-1}, respectively, due to the slightly decrease of oxidizability of ·OH under alkaline conditions [43]. Meanwhile, studies have shown that DDVP becomes more active and prone to hydrolysis under alkaline conditions than under neutral conditions, depending on its pK_a value [39]. The degradation of AZX on HiPIMS-PtTi30 anode was also carried out under different current densities. The variation of AZX removal efficiency against reaction time is shown in Fig. S4 in Supporting information, as well as the kinetic parameters (Table S6 in Supporting information). When the current density increases from 6 mA/cm^2 to 60 mA/cm^2, the degradation efficiency of AZX raised from 3.89 min^{-1} to 41.81 min^{-1} in 1 h. The removal efficiency reaches 91% as well. Obviously, the yields of reactive oxygen species (ROS) are reinforced dramatically under higher exchange current density [23]. The energy consumption of AZX increases with the increase of the current density within 6–48 mA/cm^2 (Fig. S4c in Supporting information). However, when the current density was 60 mA/cm^2, the energy consumption dropped, due to the lower power applied to the degradation of AZX [39]. AZX cyclic electrolysis experiment was carried out on the four anodes to test stability of Pt/Ti anode (Fig. S5 in Supporting information). Although the Pt coating of EP-PtTi spalled in different degrees after the strengthening life test, the catalytic effect did not fluctuate greatly.

The electron spin-resonance spectroscopy (ESR) for ROS generated during the electrocatalysis reaction is shown in Fig. 3a. There was not only 4-oxo-2,2,6,6-tetramethyl-1-peridinoxy (TEMPO) pro-

duced by $^1O_2$ in the system but also the production of $^{\bullet}OH$. The peak strength ratio of $^{\bullet}OH$ was 1:2:2:1, corresponding to the spin adduct DMPO-$^{\bullet}OH$ [44]. Also, $^{\bullet}O_2^-$ was captured by DMPO in methanol solution, and six typical peaks of DMPO-$^{\bullet}O_2^-$ signal appeared on ESR. Therefore, it can be assumed that ROS in the electrocatalysis system mainly included $^{\bullet}OH$, $^1O_2$ and $^{\bullet}O_2^-$, acting together to degrade the typical pesticide in water. The production of $^{\bullet}OH$ on the surface of four Pt/Ti anodes was measured. As shown in Fig. 3b, the yield of $^{\bullet}OH$ concentration prepared by magnetron sputtering (HiPIMS-PtTi30, HiPIMS-PtTi120) was higher than that by electroplating (EP-PtTi30, EP-PtTi120). When the current density was 60 mA/cm^2, the cumulative concentration on each anode within 30 min conformed to the quasi-zero order reaction kinetics [44].

In an electrocatalytic reaction, the formation process of $^{\bullet}O_2^-$ is relatively complex, mainly concluding two reactions. One reaction is $^{\bullet}OH$ and H_2O molecules are anodically adsorbed and oxidized to form $^{\bullet}OH$ (Eq. 1), then the quenching reaction between $^{\bullet}OH$ takes place to form $^{\bullet}O_2^-$ (Eq. 2) [45]. The other is the reduction of O_2 adsorbed on cathode to generate $^{\bullet}O_2^-$ (Eq. 3) [44]. Therefore, the production of $^{\bullet}O_2^-$ does not conform to the pseudo-first-order kinetics. Fig. 3c shows that $^{\bullet}O_2^-$ was produced in all four electrocatalysis systems, and the yield efficiency fluctuated. Meanwhile, the $^1O_2$ concentrations on the four anodes gradually decreased with reaction processing (Fig. 3d) due to the furfural alcohol was destroyed by the stronger oxidants than $^1O_2$.

In a Pt/Ti electrocatalysis reaction, $^{\bullet}OH$ has the strongest oxidation capacity, which plays a dominating role in the electrocatalytic degradation of pesticide pollutants [46]. Based on the identification of intermediates, DDVP can be transformed into trimethyl phosphate, formic acid and acetic acid, and then these intermediates will be further decomposed into small molecular inorganic substances [47]. There are four main reaction pathways (Fig. 4a), where pathways 2 and 4 are direct oxidation. The anodic adsorption of DDVP occurs redox reaction through electrons gain and loss. Pathways 1 and 3 are indirect electrocatalytic oxidation processes dominated by $^{\bullet}OH$. DDVP is eventually degraded into inorganic small molecules such as CO_2, H_2O, PO_4^{3-}.

$$OH^- + H_2O - 2e^- \rightarrow 2^{\bullet}OH + H^+ \quad (1)$$

$$^{\bullet}OH + {}^{\bullet}OH - e^- \rightarrow {}^{\bullet}O_2^- + 2H^+ \quad (2)$$

$$O_2 + e^- \rightarrow {}^{\bullet}O_2^- \quad (3)$$

AZX is structurally stable and requires a high positive potential to launch the redox reaction [47]. The degradation of AZX is mainly through the oxidation of aromatics and alkylaromatics, that is, the solvent in the system promotes the nucleophilic attack of electron-deficient carbon atoms, which leads to the formation of substitution products. Fig. 4b shows two main possible mechanisms. Firstly, AZX loses electrons to form radicals (pathways 1 and 2 take place at different reaction sites). By reacting with proton (H^+), radicals are formed and the formation of carbocation is promoted [48]. In the presence of polar solvents, the carbocation is vulnerable to nucleophilic attack, generating four intermediate products. Some intermediates may exist stably in the system, and others may be further oxidized to small molecules [47,49].

In summary, the catalytic degradation activity of Pt/Ti anodes prepared by magnetron sputtering method for DDVP and AZX is significantly better than those prepared by electroplating. Evidentially, the k_{ENR} of HiPIMS-PtTi30 anode for DDVP and AZX was 35.7 min^{-1} and 41.3 min^{-1}, higher than that on EP-Pt/Ti by 2.46 and 3.47 times, respectively. Ti substrate is also firmly bonded with Pt coating, which results in more adsorption sites for −OH under polarization conditions, and higher production of hydroxyl radical ($^{\bullet}OH$). Based on the analyses of the degradation mechanism of DDVP and AZX, two reaction pathways involving direct oxidization, indirect oxidization, electron transfer, and hydrolysis are proposed.

Declaration of competing interest

The authors declare that they have no known competing financial interests or personal relationships that could have appeared to influence the work reported in this paper.

Acknowledgments

This work was supported by National Natural Science Foundation of China (No. 21777009), Beijing Natural Science Foundation (No. 8182031).

Supplementary materials

Supplementary material associated with this article can be found, in the online version, at doi:10.1016/j.cclet.2022.01.031.

References

[1] M.J. Cerejeira, P. Viana, S. Batista, et al., Water Res. 37 (2003) 1055–1063.
[2] C. Wu, T. Li, D. Li, et al., Chin. Chem. Lett. 32 (2021) 2174–2178.
[3] S.Y. Foong, N.L. Ma, S.S. Lam, et al., J. Hazard. Mater. 400 (2020) 123006.
[4] B. Zhou, X. Kong, S. Vanka, et al., Nat. Commun. 9 (2018) 3856.
[5] C. Ju, H. Zhang, S. Yao, et al., J. Agric. Food Chem. 67 (2019) 6691–6699.
[6] G. Chen, G. Liu, H. Jia, et al., Food Chem. 362 (2021) 130118.
[7] S.H. Lin, C.T. Shyu, Water Res. 32 (1998) 1059–1066.
[8] B. Balci, N. Oturan, Water Res. 43 (2009) 1924–1934.
[9] J. Liu, W. Hu, C. Zhong, et al., J. Power Sources 223 (2013) 165–174.
[10] X. Duan, W. Wang, Q. Wang, et al., Chemosphere 260 (2020) 127587.
[11] S.A. Alves, T.C.R. Ferreira, N.S. Sabatini, et al., Chemosphere 88 (2012) 155–160.
[12] H. Zazou, N. Oturan, H. Zhang, et al., Sustainable Environ. Res. 27 (2017) 15–23.
[13] P. Alulema-Pullupaxi, L. Fernández, A. Debut, et al., Chemosphere 278 (2021) 130488.
[14] J. Qu, X. Zhao, Environ. Sci. Technol. 42 (2008) 4934–4939.
[15] D. Maharana, Z. Xu, J. Niu, et al., Chemosphere 136 (2015) 145–152.
[16] C. Zhou, Y. Wang, J. Chen, et al., Sci. Total Environ. 688 (2019) 75–82.
[17] L. Xu, S. Tang, K. Wang, et al., Chemosphere 241 (2020) 125058.
[18] C. Wang, Y. Yu, L. Yin, et al., Chemosphere 163 (2016) 584–591.
[19] X. Li, H. Xu, W. Yan, et al., J. Electroanal. Chem. 775 (2016) 43–51.
[20] X. Guo, G. Zhang, Q. Li, et al., Energy Stor. Mater. 15 (2018) 171–201.
[21] R. Subbaraman, D. Tripkovic, K.C. Chang, et al., Nat. Mater. 11 (2012) 550–557.
[22] A. Ansari, D. Nematollahi, Appl. Catal. B: Environ. 261 (2020) 118226.
[23] M. Iqbal, Y. Bando, Z. Sun, et al., Adv. Mater. 33 (2021) e2004554.
[24] C. Rakousky, U. Reimer, K. Wippermann, et al., J. Power Sources 326 (2016) 120–128.
[25] M.K. Jeon, P.J. McGinn, J. Power Sources 195 (2010) 2664–2668.
[26] Y. Sun, S. Cheng, Z. Mao, et al., Chemosphere 239 (2020) 124715.
[27] A. Moll, J.J. Blandin, R. Dendievel, et al., Surf. Coat. Technol. 415 (2021) 127130.
[28] Y. Ma, L. Li, J. Qian, et al., Energy Stor. Mater. 39 (2021) 203–224.
[29] R. Solmaz, B.D. Karahan, J. Alloys Comp. 872 (2021) 159594.
[30] C. Wang, Y. Liu, T. Zhou, et al., Chin. Chem. Lett. 30 (2019) 2231–2235.
[31] M. Ciobanu, G. Petcu, E.M. Anghel, et al., Appl. Catal. A: General 619 (2021) 118123.
[32] C. Roth, M. Goetz, H. Fuess, J. Appl. Electrochem. 31 (2001) 793–798.
[33] R.J. Watts, M. Ahmad, A.K. Hohner, et al., Water Res. 133 (2018) 247–254.
[34] L. Casanova, M.La Padula, M. Pedeferri, et al., Electrochim. Acta 379 (2021) 138190.
[35] M. Sun, Y. Wang, C. Sun, et al., Chin. Chem. Lett. 33 (2022) 385–389.
[36] Q. Zhang, M. Zhou, G. Ren, et al., Nat. Commun. 11 (2020) 1731.
[37] Q. Zhang, X. Tan, N.M. Bedford, et al., Nat. Commun. 11 (2020) 4181.
[38] J. Senthilnathan, S.A. Younis, E.E. Kwon, et al., J. Hazard. Mater. 400 (2020) 123323.
[39] Y. Wang, J. Chen, J. Gao, et al., Sep. Purif. Technol. 272 (2021) 118884.
[40] B. Huang, C. Qi, Z. Yang, et al., J. Catal. 352 (2017) 337–350.
[41] J. Li, Z. Xiong, Y. Yu, et al., Appl. Catal. B: Environ. 298 (2021) 120506.
[42] K. Liu, J.C. Yu, H. Dong, et al., Environ. Sci. Technol. 52 (2018) 12667–12674.
[43] J.E. Nutting, M. Rafiee, S.S. Stahl, Chem. Rev. 118 (2018) 4834–4885.
[44] N.L. Weinberg, H.R. Weinberg, Chem. Rev. 68 (1968) 449–523.
[45] Z. Xiong, J. Li, Y. Li, et al., J. Hazard. Mater. 406 (2021) 124725.
[46] J. Li, Y. Li, Z. Xiong, et al., Chin. Chem. Lett. 30 (2019) 2139–2146.
[47] E. Mpofu, A. Alias, K. Tomita, et al., Chemosphere 273 (2021) 129663.
[48] M. Gautam, T. Etzerodt, I.S. Fomsgaard, Int. J. Environ. Anal. Chem. 97 (2017) 419–430.
[49] F. Cao, P. Wu, L. Huang, et al., Aquatic. Toxicol. 198 (2018) 129–140.